Published in final edited form as:
Ultramicroscopy. 2014 November ; 146: 33–38. doi:10.1016/j.ultramic.2014.05.004.

Analysis of electron beam damage of exfoliated MoS_2 sheets and quantitative HAADF-STEM imaging

A. Garcia[1,†], **A.M. Raya**[2], **M.M. Mariscal**[3], **R. Esparza**[1,‡], **M. Herrera**[2], **S.I. Molina**[2], **G. Scavello**[4], **P.L. Galindo**[4], **M. Jose-Yacaman**[1], and **A. Ponce**[1,*]

[1]Department of Physics and Astronomy, University of Texas at San Antonio. One UTSA Circle, San Antonio, TX 78249, USA

[2]Departamento de Ciencia de los Materiales en Ingeniería Metalúrgica y Química Inorgánica, Universidad de Cádiz, 11510 Puerto Real, Cádiz, Spain

[3]INFIQC-CONICET, Departamento de Matemática y Física, Facultad de Ciencias Químicas, Universidad Nacional de Córdoba, XUA5000 Cordoba, Argentina

[4]Departamento de Ingeniería Informática, CASEM, Universidad de Cádiz, Campus Río San Pedro, Puerto Real, 11510 Cádiz, Spain

Abstract

In this work we examined MoS_2 sheets by aberration-corrected scanning transmission electron microscopy (STEM) at three different energies: 80, 120 and 200 kV. Structural damage of the MoS_2 sheets has been controlled at 80 kV according a theoretical calculation based on the inelastic scattering of the electrons involved in the interaction electron-matter. The threshold energy for the MoS2 material has been found and experimentally verified in the microscope. At energies higher than the energy threshold we show surface and edge defects produced by the electron beam irradiation. Quantitative analysis at atomic level in the images obtained at 80 kV has been performed using the experimental images and via STEM simulations using SICSTEM software to determine the exact number of MoS_2 layers.

Keywords

low-voltage transmission electron microscopy; aberration-corrected microscopy; molybdenum disulfide; radiation damage

*Corresponding author. Tel.:+1 210 458 8267. arturo.ponce@utsa.edu (A. Ponce).
†Current address: Centro de Investigación en Materiales Avanzados S.C., Alianza Norte 202, Apodaca Nuevo León, 66600, Mexico.
‡Current address: Centro de Física Aplicada y Tecnología Avanzada, Universidad Nacional Autónoma de México, Boulevard Juriquilla 3001, Santiago de Querétaro, 76230, Mexico.

1. Introduction

Tunability of electronic bandgap engineering in semiconductor materials is a research field permanently open in optoelectronics and energy harvesting. At the present, conventional III-V or II-VI semiconductors bandgap can be optimized accurately from ultraviolet to infrared radiation by doping of chemical elements. Furthermore, nanostructured semiconductors exhibit variations that largely are determined by a quantum confinement linked to the decreasing size of nanostructures [1]. In addition, a size reduction in nanostructures, such as silicon or germanium, leads to transformation from indirect to direct bandgap [2-3]. In this way, recent developments in 2D few-layered crystals have demonstrated that the electronic bandgap is tunable and shifted [4-7]. Sulfide semiconductors, including copper-containing sulfide materials have remarkable applications in photovoltaic conversion [8-10]. Metal dichalcogenides (MX_2) have increased relevantly their importance in applications as semiconductor materials focused in the high charge carrier mobility [11-12], besides the catalytic and lubricant applications and other interesting properties [13-14]. MoS_2 monolayer is a direct band-gap semiconductor unlike its bulk nature at 1.2 eV [15], as a consequence a remarkable increase in luminescence is experimentally measured [16]. For energy harvesting applications, the maximum efficiency energy conversion, from the incident light to the photogenerated electron-holes pairs, ranges from 1 to 2 eV in the bandgap [17]. It has become clear that MoS_2, and other metal dichalcogenides with a narrow bandgap, are great candidate materials for new photovoltaic applications. Unlike graphene, in which a monolayer corresponds to a semimetal with no bandgap [18], one single layer molybdenum disulfide (S-Mo-S) becomes as a direct bandgap material. Metal dichalcogenides exhibit a band gap shift from indirect to direct as a function of the number of S-Mo-S slabs (N) and increasing the bandgap from the bulk value up to 0.6 eV for a single MoS_2 layer [6-7].

The imaging at atomic resolution of few-layered crystals represents a challenge due to their high sensitivity to the electron beam irradiation causing an irreversible damage in their crystalline structure. This structural damage induced by the electron beam is mainly caused by three different mechanisms: radiolysis, heating and knock-on [20-21]. The first one involves bond-breaking and it is expected to play a key role in isolators and some semiconductors. The second mechanism is related to the inelastic scattering between the electrons coming from the beam and the atomic electrons.

In 2D crystals the electron beam may cause damage in the surface and edges [22] of the extended sheets, producing irregular edges or holes caused by a high electron beam penetration. Particularly there are recent papers in which the radiation damage in MoS_2 sheets by graphene encapsulation [23-24]. However, the mechanisms of radiation damage are extremely sensitive to the environment [25] and as consequence to the radiation damage. Zan et al [23] and Algara-Siller [24] show evidence of radiation damage in MoS_2 layers obtained by polymerbased wet-transfer methods which produces a different chemical environment since hydrocarbides can affect the radiation mechanism. On the other hand the beam current plays a critical role in the control of radiation damage.

In the present work, we calculated the optimum threshold energy used in the microscope in which the Mo-S bonding is stable. Experimentally we worked at three different energies (80, 120 and 200 kV) and found that the damage is reduced according with the theoretical prediction. In addition, a methodology based on the quantification of the integrated intensities around each atomic column was applied to determine the number layers of MoS_2 sheets obtained by lithium intercalation exfoliation method, which produces a stable and free of hydrocarbides environments for their electron microscopy analyses. This methodology was applied to atomic resolution images registered by aberration-corrected scanning transmission electron microscopy (STEM) collected in a high angle annular dark field (HAADF) detector.

2. Theoretical calculation

In MoS_2 the structural damage induced by the electron beam irradiation is associated to heating and knock-on. However, the temperature rise due to this effect has been shown to be negligible for beam diameters and electron dose used in the present work, see ref. [19]. The inelastic scattering of the electrons involved, electron beam and electron of the atoms, produces atomic displacements (bulk and surface ones). The maximum energy transferred (E_{max}) to an atomic nucleus with mass M is calculated as follow (including exact relativistic kinematics):

$$E_{\max}=\frac{E_{\text{beam}}\ (E_{\text{beam}}+2m_e c^2)}{E_{\text{beam}}+(1+m_e/M)^2 Mc^2/2}$$

Where E_{beam} is the incident electron beam energy, m_e the electron mass at rest, and c the speed of light. E_{max} as a function of the incident electron energy is shown in Fig. 1 for both atoms Mo and S. The maximum transferred energy increases linearly as the incident electron energy. At the same time at a given incident electron energy, E_{max} decreases with the atomic mass, indicating that lighter atoms will need less energy to be displaced by the electron beam. It is important to mention that if E_{max} exceeds the displacement energy E_d (marked in the graph Fig. 1) which is particular for each element, the electron beam can move bulk atoms from their lattice position and even more, and also it is possible take away atoms from the surface of the sample. E_d values for Mo and S has been taken form Ref. [26]. If we observe the maximum transferred energy at an operation voltage of 200 kV for sulfur nuclei (red dash dotted lines), it is appreciably larger than the threshold energy E_d (S) (red dotted line) and therefore, S atoms at 200 kV will be displaced by the knock-on mechanism. The case of Mo is different because at 200 kV the threshold energy E_d (Mo) (black dotted line) is considerably larger than the maximum displacement energy. The situation for (S) is reverted at incident electron energies lower than 100 kV, for instance at 80 kV, where threshold energies are lower than the maximum displacement energy and consequently surface sputtering is not expected. In this way, the best the optimum incident electron energy is 80 kV.

3. Experimental

The MoS_2 (99% Aldrich) was soaked in a 1.6M solution of n-butyl lithium in hexane (Aldrich) to intercalate the lithium, which acts as a strong reducing agent and generates intercalation compounds containing the Li+ intercalated. This reaction should be carried out into an inert atmosphere for 48 hours. Following the intercalation of the MoS_2 by lithium, the MoS_2 was washed in hexane several times. After is dried and sealed in a vial [27]. The intercalated sample was exfoliated by ultrasonication with distilled water in a closed vial for 5 hours, during which hydrogen gas was formed between layers, and the expansion of this gas tends to separate the MoS_2 layers by loss of periodicity along the *c* axis. The layers become separate completely and remain suspended in the aqueous solution per 1 week approximately. Moreover, the insertion of organic materials within layers avoids the re-stacking and generates stable dispersions. For the electron microscopy analysis, a drop of the suspension was deposited onto a holey carbon grid. The atomic resolution images were obtained using an aberration-corrected scanning transmission electron microscope JEOL ARM 200F. The probe size used for acquiring the HAADF-STEM images was 9C (23.2 pA), and the CL aperture size was 40 μm. HAADF STEM images were acquired with a camera length of 8 cm. The images were collected at three different energies 80, 120 and 200 kV used in the theoretical calculations. The microscope has been optimized to work at low energies by a proper alignment of the CEOS GmbH probe-corrector. In accordance with the irradiation electron energies calculated in the previous section, when the microscope is operated at 120 and 200 kV the sample exhibits structural damages (see Fig. 1). The experimental evidence of this damage is showed in the Fig. 2, in which surface damage is registered in the HAADF-STEM images recorded in the center of the 2D sheets at 120 kV (Fig 2a) and 200 kV (Fig. 2b). In addition, an edge of the sample was also evaluated at 120 kV as function of scanning time, initially (first scanning) with a structure (Fig. 2c) deteriorated after 240 seconds of continuous scanning Fig. 2d. It is clearly observable the structure change from the initial scanning and after the last one (240 s), these changes have been indicated with filled circles above the arrows traced in the figures 2c and 2d. Electron beam irradiation damage has not been observed at 80 kV, which is consistent with the theoretical calculation described previously.

4. Quantitative analysis

The quantitative analysis has been performed in the images collected at 80 kV in which the sample is stable under the electron beam irradiation and no structural damage has been observed. The images taken using aberration-corrected HAADF-STEM mode show a contrast of individual molybdenum and sulfur atoms distinguished clearly, which is typically named Z-contrast imaging [32]. In MoS_2 sheets, the HAADF-STEM images are collected in the [001] zone axis and considering the case of one-single layer (S-Mo-S) a hexagonal lattice is observed. In order to quantify the number of layers present in the sample, HAADF-STEM simulated images of MoS_2 sheets have been computed using the software SICSTEM [28]. The simulations have been carried out using the experimental parameters the microscope: $Cs = 7.431\times10^{-4}$ mm and $C_5 = 0$ mm, objective aperture of 27 mrad and an inner and outer annular detector angles of 33 and 125 mrad, respectively ($\sim$ 23 pA). This software runs in a 256-parallel Xenon cluster which allows an improvement of

approximately 350 times in processing time comparing to a single-node machine. Thermal diffuse scattering (TDS) is considered in the calculation of the intensities of the object exit plane by the multislice method and using a TDS absorptive potential approach. Spatial incoherence of the electron beam in the microscope has been considered in the simulations. In this way, a series of images were obtained through the convolution of those images using computed Gaussian functions with different standard deviations. The simulated images were compared with the experimental ones using a function based in the Fourier space [29]. The obtained results are valid for the considered microscope working in the same conditions, and are independent of the analyzed sample.

Fig. 3a shows a high resolution HAADF-STEM experimental image obtained from the MoS_2 sample. We have applied a Wiener filter to this image in order to reduce the noise. As it can be observed, two different atomic columns can be distinguished in the image, the most intense corresponding to Mo atoms (Z=42) and the less intense to S toms (Z=16). A simulated images were obtained using the software SICSTEM [28] and a good matching is observed in the Fig.3b, in which two layers have been used. The case of one, two and three layers has been simulated as well. As can be observed in figure 4a, which corresponds a one MoS_2 layer, the image contrast corresponding to S atoms is very weak (virtually unnoticed) in comparison with the strong brightness corresponding to Mo atoms, this is due to the large difference in atomic number of both elements (Mo=42 and S=16). This figure is not in agreement with the experimental HAADF-STEM image, therefore is necessary to increase the amount of layers in the calculations. Figure 4b shows the simulated HAADF-STEM images of two MoS_2 layers. The image corresponds to one unit cell of the MoS_2-2H structure with c axis equal to 1.229 nm. The obtained image contrast of this image is different than found in the figure 3a. In this case the brightness contrast of the S atoms is appreciable, and it is clear that each hexagonal ring consists of three Mo atoms and three S atoms. This figure is almost in agreement with the experimental HAADF-STEM image. Finally, figure 4c shows the simulated HAADF-STEM image corresponding to four MoS_2 layers (two unit cells) with c axis equal to 2.458 nm. From the image it is clear that the image contrast is almost the same all over the image, therefore, increasing the numbers of layers or the unit cells, the found brightness contrast will be almost similar and the Mo and S atoms are not distinguished. In order to being able to compare these experimental results to the simulated images, it is necessary to average the intensity over a significant number of atomic columns. For this, we have used a method for measuring the integrated intensities around each atomic column [29] that has been successfully used previously for the calculation of the composition of different semiconductor materials from experimental HAADF-STEM image [31-32]. In the case of more than one MoS_2 layers, the crystal can be considered as its bulk crystalline structures, in which a layer-stacked of S-Mo-S units are repeated following two main trigonal phases: the first one is a trigonal-prismatic 2H and the second one is a rhombohedral structure, also called 3R-MoS_2 [33-34]. Rhombohedral structure differs from the 2H by the stacking layers of each slab S-Mo-S. 2H structure is stacked in an anti-parallel orientation whereas rhombohedral stacking is self-assembled oriented. As a consequence of the two different stacking MoS_2 layers, the projection along the [001] direction corresponds to a parallelepipedon for the rhombohedral and a hexagonal arrangement for the trigonal-prismatic. These two structures were considered for the

simulations in order to extract the quantitative number of layers and are showed in the Fig. 4c considering the 2H structure and the case for one, two and four layers. The direct matching of experimental and simulated HAADF-STEM images is carried out by the image contrast comparison of intensity profiles determined across the Mo-S atomic columns. The black curve shows the intensity profile from the experimental HAADF-STEM image, this will serve as a reference point. The red curve shows the intensity profile of the simulated HAADF-STEM image of one MoS_2 layer. The peak corresponding to the Mo has the same intensity compared with the experimental curve; however, the peak of S is very different due to weak intensity brightness contrast. The blue curve corresponding to the intensity profile of the HAADF-STEM image with two MoS_2 layers (1 unit cell). The ratio between Mo and S intensities profiles peaks is consistent with the experimental image. Therefore, we could assume that the experimental MoS_2 image corresponds to a 2 layers structure. Finally, the green curve corresponding to the intensity profile of the HAADF-STEM image with four MoS_2 layers (2 unit cells). As can be observed, the intensity profile of the Mo peak decrease compared with the experimental profile, and the intensity profile of the S peak increases. It can be concluded that increasing the number of MoS_2 unit cells, the brightness of the atomic columns will be similar. As it can be observed, there is a good agreement between the intensity obtained from the experimental images and from the simulations.

5. Conclusion

Aberration-corrected scanning transmission electron microscopy has been used to obtain atomic resolution images using three different energies, 80, 120 and 200 kV. The optimum energy to avoid any structural damage in MoS_2 sheets caused by the electron beam irradiation has been calculated and shows that below 80 kV the sample is stable. The quantitative method for determining the number of layers has been successfully applied by comparison of simulated images with the experimental ones.

Acknowledgments

This project was supported by grants from the National Center for Research Resources (5 G12RR013646-12) and the National Institute on Minority Health and Health Disparities (G12MD007591) from the National Institutes of Health. The authors would like to acknowledge to the NSF for support with grants DMR-1103730, “Alloys at the Nanoscale: The Case of Nanoparticles Second Phase and PREM: NSF PREM Grant # DMR 0934218. AR and SIM acknowledge the support from the Spanish MINECO (projects TEC2011-29120-C05-03 and CONSOLIDER INGENIO 2010 CSD2009-00013) and the Junta de Andalucía, (PAI research group INNANOMAT, ref. TEP-946). M.M.M. acknowledges support from CONICET (CIAM-Program), ANPCyT (PICT2010/1233) and Universidad Nacional de Cordoba.

References

1. Alivisatos P. Semiconductor Clusters, Nanocrystals, and Quantum Dots. Science. 1996; 271:933–937.
2. Nolan M, OCallaghan S, Fagas G, Greer JC, Frauenheim T. Silicon Nanowire Band Gap Modification. Nano Lett. 2007; 7:43–38.
3. Liang D, Bowers JE. Recent progress in lasers on silicon. Nature Photonics. 2010; 4:511–517.
4. Schwierz F. The rise and rise of graphene. Nature Nanotech. 2010; 5:487–496.
5. Zhang Y, Tang T, Girit C, Hao Z, Martin MC, Zettl A, Crommie MF, Shen YR, Wang F. Direct observation of a widely tunable bandgap in bilayer graphene. Nature. 2009; 459:820–823. [PubMed: 19516337]

6. Mak KF, Lee C, Hone J, Shan J, Heinz TF. Atomically Thin MoS_2: A New Direct-Gap Semiconductor. Phys Rev Lett. 2010; 105:136805. [PubMed: 21230799]
7. Radisavljevic B, Radenovic A, Brivio J, Giacometti V, Kis A. Single-layer MoS_2 transistors. Nature. 2011; 6:147–150.
8. Braga A, Gimenez S, Concina I, Vomiero A, Mora-Sero I. Panchromatic Sensitized Solar Cells Based on Metal Sulfide Quantum Dots Grown Directly on Nanostructured TiO_2 Electrodes. J Phys Chem Lett. 2011; 2:454–460.
9. Tang J, Huo Z, Brittman S, Gao H, Yang P. Nature Nanotech. 2011; 6:568–572.
10. Page M, Niitsoo O, Itzhaik Y, Cahen D, Hodes G. Copper sulfide as a light absorber in wet-chemical synthesized extremely thin absorber (ETA) solar cells. Energy Environ Sci. 2009; 2:220–223.
11. Ohuchi FS, Jaegermann W, Pettenkofer C, Parkinson BA. Semiconductor to metal transition of WS_2 induced by K intercalation in ultrahigh vacuum. Lagmuir. 1989; 5:439–442.
12. Podzorov V, Gershenson ME, Kloc Ch, Zeis R, Bucher E. High-mobility field-effect transistors based on transition metal dichalcogenides. Appl Phys Lett. 2004; 84:3301.
13. Wang HD, Xu BS, Liu JJ, Zhuang DM. The friction-reduction model of the iron sulfide film prepared by plasma source ion sulfuration. Surf Coat Technol. 2007; 201:6719–6722.
14. Okamoto Y, Kato A, Usman, Rinaldi N, Fujikawa T, Koshika H, Hiromitsu I, Kubota T. Effect of sulfidation temperature on the intrinsic activity of Co–MoS_2 and Co–WS_2 hydrodesulfurization catalysts. J Catal. 2009; 265:216–228.
15. Kam KK, Parkinson BA. Detailed Photocurrent Spectroscopy of the Semiconducting Group V I Transition Metal Dichaicogenldes. J Phys Chem. 1982; 86:463–467.
16. Eda G, Yamaguchi H, Voiry D, Fujita T, Chen M, Chhowalla M. Photoluminescence from Chemically Exfoliated MoS_2. Nano Lett. 2011; 11:5111–5116. [PubMed: 22035145]
17. Green, MA. Solar cells: operating principles, technology, and system applications. Perntice-Hall; Upper Saddle River (NJ): 1982.
18. Yacoby A. Graphene: Tri and tri again. Nature Physics. 2011; 7:925–926.
19. Egerton RF, Li P, Malac M. Radiation damage in the TEM and SEM. Micron. 2004; 35:399–409. [PubMed: 15120123]
20. Egerton RF, McLeod R, Wang F, Malac M. Basic questions related to electron-induced sputtering in the TEM. Ultramicroscopy. 2010; 110:991–997.
21. Meyer JC, Eder F, Kurasch S, Skakalova V, Kotakoski J, Park HJ, Roth S, Chuvilin A, Eyhusen S, Benner G, Krasheninnikov AV, Kaiser U. Accurate Measurement of Electron Beam Induced Displacement Cross Sections for Single-Layer Graphene. Phys Rev Lett. 2012; 108:196102. [PubMed: 23003063]
22. Han SW, Kwon Hyuksang, Kim Seong Keun, Ryu Sunmin, Yun Won Seok, Kim DH, Hwang JH, Kang JS, Baik J, Shin HJ, Hong SC. Band-gap transition induced by interlayer van der Waals interaction in MoS_2. Phys Rev B. 2011; 84:045409.
23. Zan R, Ramasse QM, Jalil R, Georgiou T, Bangert U, Novoselov KS. Control of Radiation Damage in MoS2 by Graphene Encapsulation. ACS Nano. 2013; 7:10167. [PubMed: 24116975]
24. Algara-Siller G, Kurasch S, Sedighi M, Lehtinen O, Kaiser U. The pristine atomic structure of MoS_2 monolayer protected from electron radiation damage by graphene. Appl Phys Lett. 2013; 103:203107.
25. Coleman JN, Lotya M, O'Neill A, Bergin SD, King PJ, Khan U, Young K, Gaucher A, De S, Smith RJ, Shvets IV, Arora SK, Stanton G, Kim HY, Lee K, Kim GT, Duesberg GS, Hallam T, Boland JJ, Wang JJ, Donegan JF, Grunlan JC, Moriarty G, Shmeliov A, Nicholls RJ, Perkins JM, Grieveson EM, Theuwissen K, McComb DW, Nellist PD, Nicolosi V. Two-Dimensional Nanosheets Produced by Liquid Exfoliation of Layered Materials. Science. 2011; 331:568–571. [PubMed: 21292974]
26. Kinsa HP, Kotakoski J, Kurasch S, Lehtinen O, Kaiser U, Krasheninnikov A. Two-Dimensional Transition Metal Dichalcogenides under Electron Irradiation: Defect Production and Doping. Phys Rev Lett. 2012; 109:035503. [PubMed: 22861869]
27. Dines MB. Lithium intercalation via n-butyllithium of the layered transition metal dichalcogenides. Mater Res Bull. 1975; 10:287–292.

28. Pizarro J, Galindo PL, Guerrero E, Yanez A, Guerrero MP, Rosenauer A, Sales DL, Molina SI. Simulation of high angle annular dark field scanning transmission electron microscopy images of large nanostructures. Appl Phys Lett. 2008; 93:153107.

29. Molina SI, Guerrero MP, Sales DL, Varela M, Pennycook SJ. Calculation of integrated intensities in aberration-corrected Z-contrast images. J Electron Microsc. 2011; 60:29–33.

30. Molina SI, Sales DL, Galindo PL, Fuster D, Gonzalez Y, Alen B, Gonzalez L, Varela M, Pennycook SJ. Column-by-column compositional mapping by Z-contrast imaging. Ultramicroscopy. 2009; 109:172–176. [PubMed: 19062188]

31. Hernandez-Maldonado, Herrera M, Alonso-Gonzalez P, Gonzalez Y, Gonzalez L, Gazquez J, Varela M, Pennycook SJ, Guerrero-Lebrero MD, Pizarro J, Galindo PL, Molina SI. Compositional Analysis with Atomic Column Spatial Resolution by 5th-Order Aberration-Corrected Scanning Transmission Electron Microscopy. Microsc Microanal. 2011; 17:578–581. [PubMed: 21615979]

32. Sales DL, Guerrero E, Rodrigo JF, Galindo PL, Yanez A, Shafi M, Khatab A, Mari RH, Henini M, Novikov S, Chisholm MF, Molina SI. Distribution of bismuth atoms in epitaxial GaAsBi. Appl Phys Lett. 2011; 98:101902.

33. Takahashi N, Shiojiri M. Stacking faults in hexagonal and rhombohedral MoS_2 crystals produced by mechanical operation in relation to lubrication. Wear. 1993; 167:163–171.

34. Du G, Guo Z, Wang S, Zeng R, Chen Z, Liua H. Superior stability and high capacity of restacked molybdenum disulfide as anode material for lithium ion batteries. Chem Commun. 2010; 46:1106–1108.

Highlights

- MoS_2 sheets were exfoliated by using hydrogen gas flow to separate the MoS_2 layers.
- The optimum energy to avoid structural damage was calculated.
- Cs-corrected STEM imaging was used to obtain atomic resolution images.
- Three energies were used in STEM imaging: 80, 120 and 200 kV.
- A quantitative method for determining the number of layers has been applied.
- The quantitative method is based on the intensity maxima located at atomic level.

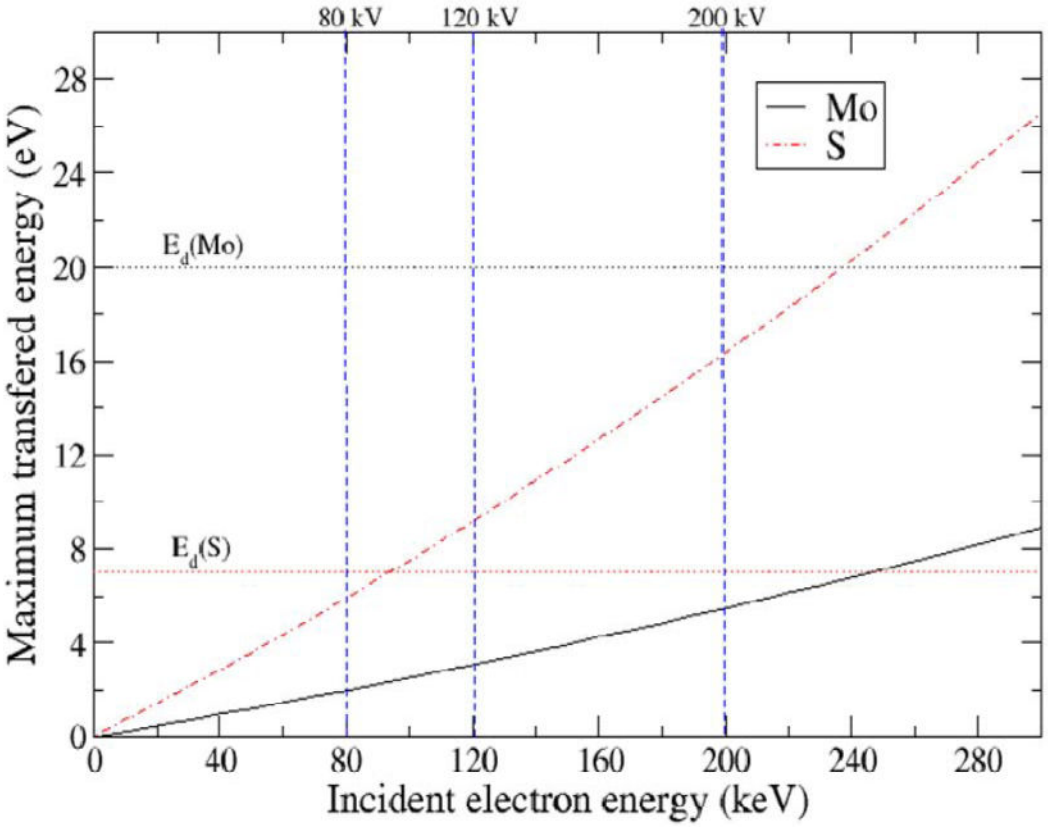

Fig. 1.

Maximum transferred energy (E_{max}) by elastic scattering for Mo and S, *vs*. the incident-electron energy.

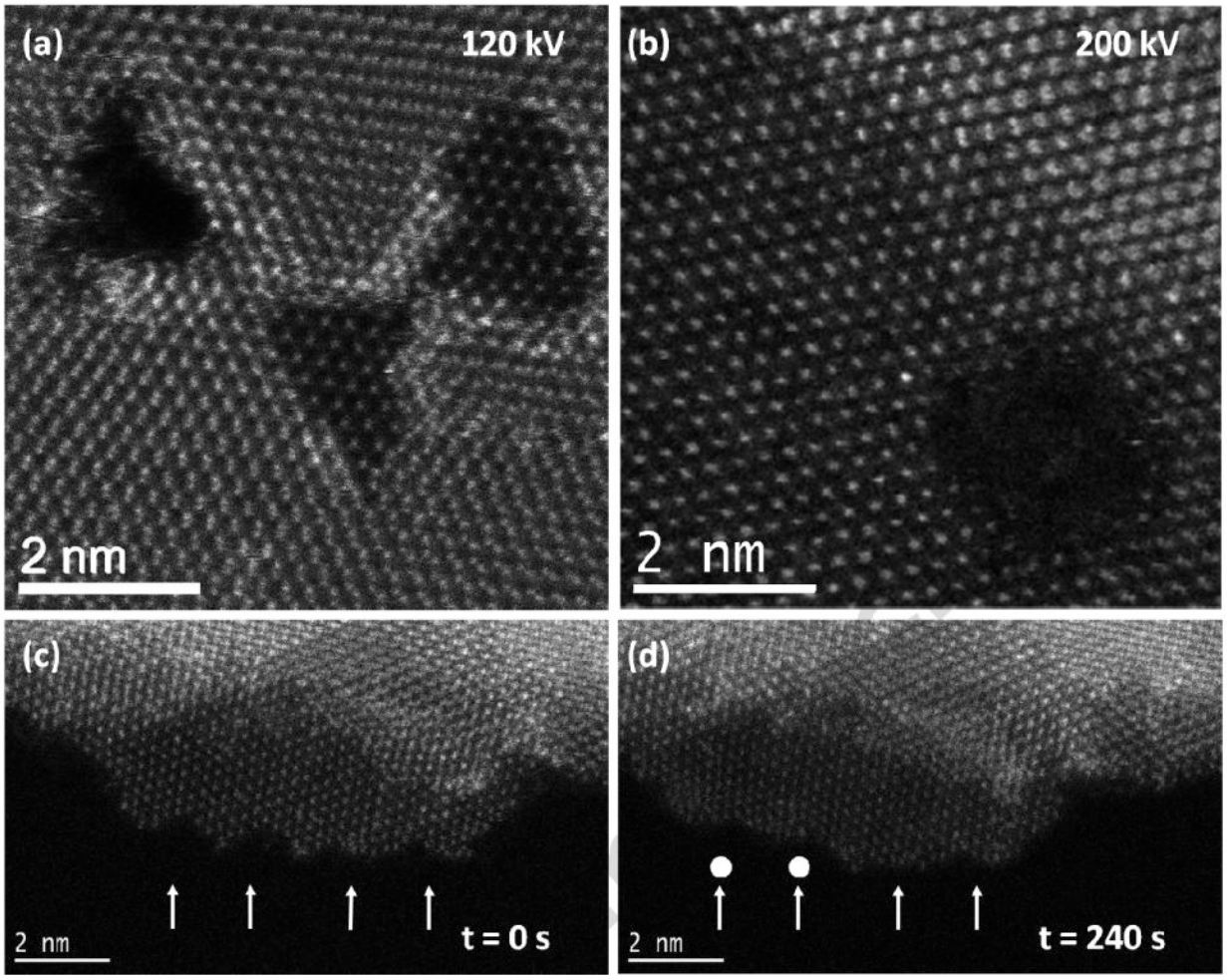

Fig. 2.

Electron beam induced damage at (a) 120 and (b) 200 kV in the surface of MoS_2 layers. Edge defects evolution from (c) the initial scanning (t = 0 s) and (d) up to 240 seconds of a continuous electron beam scanning at 120 kV.

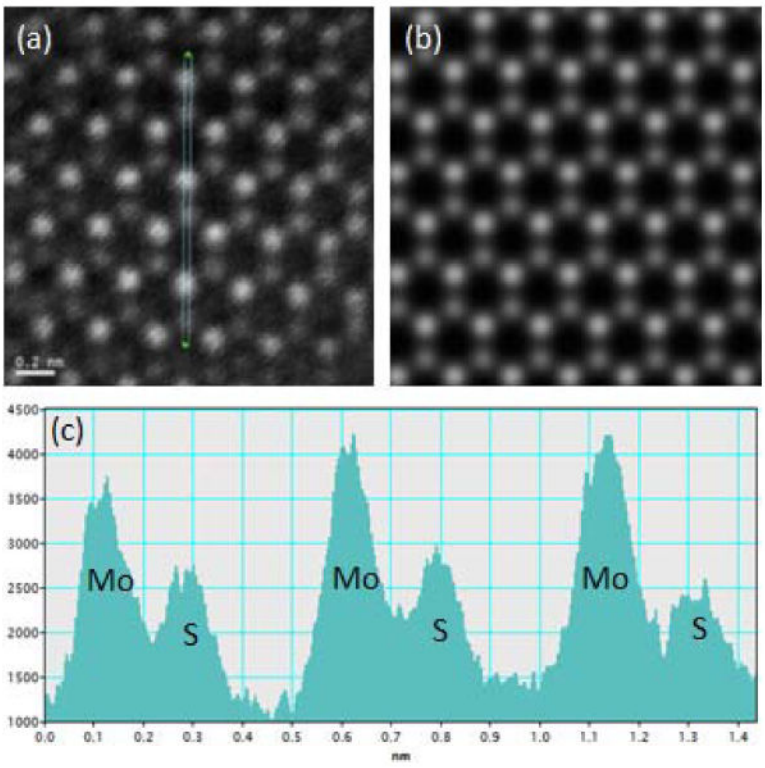

Fig.3.

(a) Experimental HAADF-STEM image of MoS_2, (c) Intensity profile along the line marked in (a), (b) Simulated HAADF-STEM images of MoS_2 using SICSTEM software using two layers.

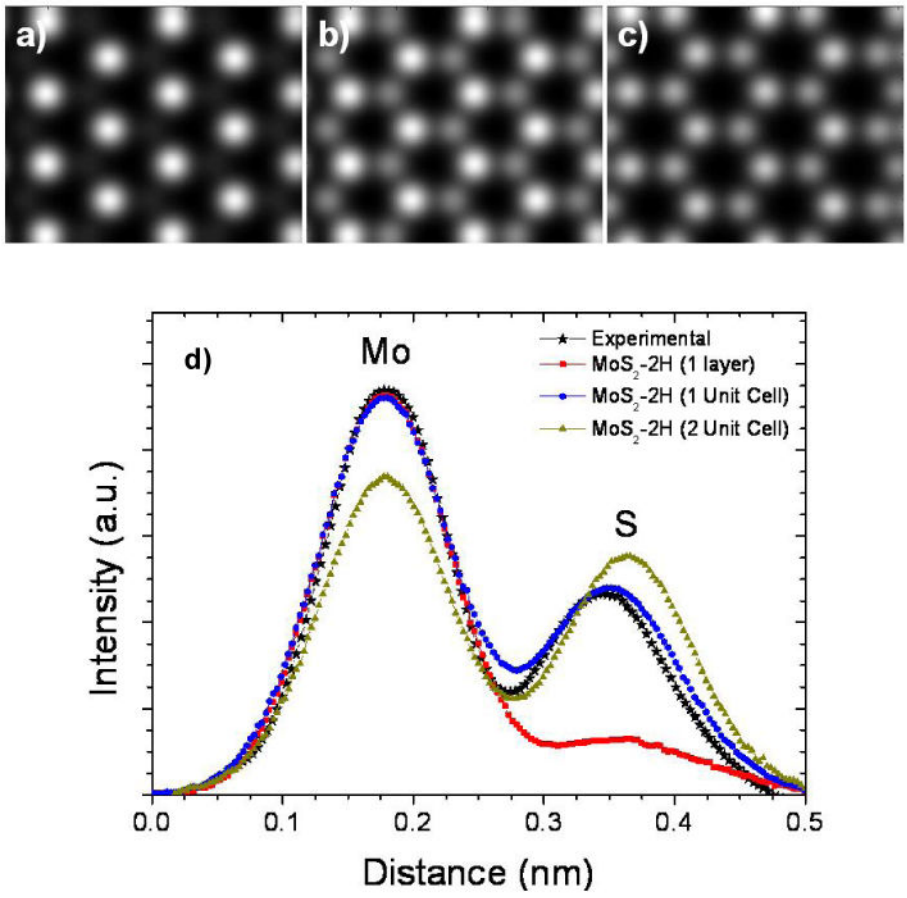

Fig.4.

Simulated HAADF-STEM images; a) one layer, b) two layers (1 unit cell) and c) four layers (2 unit cells) of MoS_2-2H structure. Note in this particular case the strong dependence of image contrast as a function of the thickness of the specimen, d) Illustration of the line profile across the Mo and S atoms of the experimental and simulated HAADF-STEM images of MoS2 specimen.